Analytical calculation of stall-inception and surge points for an axial-flow compressor rotor

Efrén M. Benavides[1]

Gregorio L. Juste

Universidad Politécnica de Madrid, Spain, Madrid 28040

Abstract: Recently, a theoretical criterion to calculate the stability of an axial-flow compressor rotor has been presented in the scientific literature. This theoretical criterion was used for determining the locus of the stability line over the rotor map and for predicting the post-stall evolution of the constant-speed line of a rotor. The main objective of this paper is to improve the predictions of such a model. To do that, the paper proposes a different characterization of the characteristic azimuthal length and a calculation of the ratio of specific heats based on a polytropic exponent. Thanks to these new values, the model predicts two bifurcation points in the behaviour of the flow: the inception point of the instability and the surge point. Experimental data from a pure axial compressor are used to validate the model showing that the prediction of the flow coefficient at the surge point has an error inferior to 5%. For the rotor studied, the paper provides a quantitative and qualitative description of the inception of the instability and of the mechanism involved in the instable region of the compressor map. The paper also discusses the role of rotor efficiency in the position of the bifurcations and gives a sensitivity analysis of its position. Finally, it presents a discussion about how the model can explain the different behaviours exhibited by the same rotor when the flow coefficient is reduced.

Keywords: axial compressor, stability, surge, stall, performance, compressor map, stability line, inception

[1] Professor, ETSI Aeronáuticos (UPM), Pza. Cardenal Cisneros 3, 28040 Madrid (Spain), efren.moreno@upm.es

I. INTRODUCTION

Due to its importance, there is a large number of articles trying to calculate the pressure rise characteristic over the entire flow-rate range of a compressor, which, indeed, requires a method for calculating or predicting the stall onset. There are methods based on analysing pressure signals from sensors [1-4], based on solving computational models [5-7], or based on analytical or engineering models [8-12]. A good review of the types of stall and surge behaviour can be found in Ref. [13].

In this article the model will be based on a previous work of the author [14] where a different description of the mean-line stability was presented based on the idea given in Ref. [11]. This model is based on a set of logical inferences that produces an analytical model taking into account the effect of the number of blades, the basic geometry, and the operational point. In order to understand this approach, it is useful to think about the azimuthal plane in Fig. 1, which represents an axial rotor with constant medium radius, variable area, negligible radial velocity component, and inlet and outlet sections with homogeneous and steady properties and velocities. In this context, Ref. [14] establishes a set of logical inferences that can be summarized by the following Stability Theorem. When a high-performance axial-flow compressor rotor works with steady and homogeneous properties at the inlet and outlet stations in a noisy environment, the necessary and sufficient condition for instability is $0<\xi<1$, where ξ is defined as:

$$\xi = \sigma_x / \Phi_{esc} \tag{1}$$

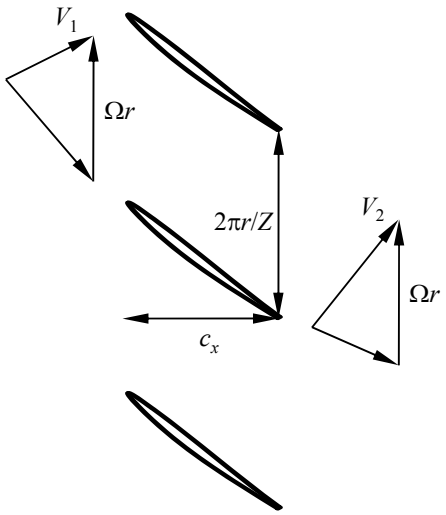

Fig.1 Inlet and outlet velocity triangles, spacing and axial chord in the two-dimensional cascade used in the model. V_1 and V_2 are respectively the inlet and outlet absolute velocities and Ωr is the blade velocity.

In this Equation, the numerator is a ratio of characteristic lengths and the denominator is a function that depends on the operational point. Refs. [16-18] estimate the coefficient σ_x as the axial solidity of the rotor, whose definition is given by Eq. (2). The denominator was obtained by Ref. [14] as a potential that measures the possibility of having escaping particles (i.e., reversed flow). Its definition is given by Eq. (3). The ratio of both in Eq. (1) is a parameter ξ that measures the possibility of having escaping particles in the inlet section of the rotor. As can be seen in Eq. (3), the potential for escaping depends on the blade speed, Ωr, the static outlet enthalpy, h_2, the static outlet and inlet pressures, P_2 and P_1, the axial and tangential components of the absolute outlet velocity, V_{x2} and $V_{\theta 2}$, and the ratio of specific heats, γ.

$$\sigma_x = \frac{Zc_x}{2\pi r} \tag{2}$$

$$\Phi_{esc} = \frac{\sqrt{2h_2\left[1-\left(\frac{P_1}{P_2}\right)^{\frac{\gamma-1}{\gamma}}\right]}-V_{x2}}{\left|\Omega r - V_{\theta 2}\right|} \tag{3}$$

A posterior study showed that the stability index in Eq. (1) could be improved [15, 16]. The result of that work was a new stability index, which is given in Eq. (4). Using this index and the Stability Theorem, i.e., using only theoretical arguments, Ref. [16] gave a calculation of the constant-speed line of an axial compressor in the surge region of the map. This constant-speed line is drawn in Fig. 2, where it is possible to appreciate the good agreement between the experimental points and the theoretical line for all the mass flow rates studied.

$$\xi_c = e^{\frac{2h_2\left[\left(\frac{P_1}{P_2}\right)^{\frac{\gamma-1}{\gamma}}-1\right]}{1+\left[V_{x2}+\sigma_x\left|V_{\theta 2}-\Omega r\right|\right]^2}} \tag{4}$$

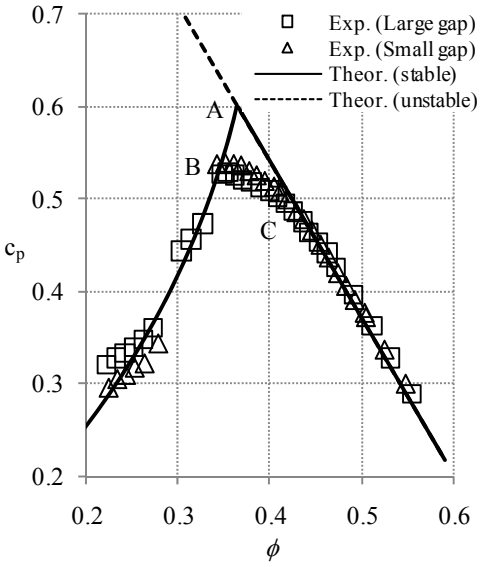

Fig. 2 Pressure coefficient as a function of the flow coefficient for a pure axial stage. The solid line is the theoretical line predicted by Ref. [16] using the Stability Theorem. The squares and triangles are the experimental points obtained from Ref [19].

The portion of the line with a positive slope was calculated thanks to the Stability Theorem. Although the agreement is quite good, there are some discrepancies. The removal of which is the main purpose of this article. As Fig. 2 shows, the result of the model (solid line) diverges from the experimental points just at point C. Although Ref. [16] gives an explanation of point C based on the stability of the stator, the behavior between points B and C is not correctly predicted. Thus, in order to reduce such discrepancies, this article tries to discover if the application of the

Stability Theorem to the rotor alone can explain the experimental results in that section of the line. To achieve this task the article is planned as follows.

First, a revision of the theory supporting the Stability Theorem and a revision of the basic equations of turbomachinery are presented. Then, two variables of the model are fed with an improved approach: one variable is the characteristic azimuthal length used to calculate the parameter σ_x in Eq. (4), and the other is the ratio of specific heats that will be calculated as a polytropic exponent. The next section uses the same low-Mach-number pure-axial rotor used by Ref. [16] for obtaining Fig. 2, whose geometry and experimental test points are given in Refs [19-21], to calibrate the basic equations of the stage. These basic equations allow us to predict the pressure rise for the region of high flow. Providing this part of the constant-speed line is known, we use the Stability Theorem to predict, without any additional adjusting parameter, the rest of the constant-speed line. Section IV predicts the position of a first bifurcation (point C in Fig. 2) and Section V performs an analysis of sensitivity. The next section studies the influence of the rotor efficiency and shows that efficiency is not the relevant parameter in the post-inception region of the constant-speed line. Section VII uses the result of the Stability Theorem to characterize the relevant geometry and gives a new calculation of the characteristic azimuthal length and outlet area. With this information, the surge point (point B in Fig. 2) is obtained as a second bifurcation with an error level in the flow coefficient less than 5 percent. With the constant-speed line theoretically calculated between points B and C, Section VII explores the prediction of the Stability Theorem for those points that are located in the surge region of the constant-speed line. Finally, a discussion based on the Stability Theorem about the post-stall evolution of the rotor and about the plausible regimens involved in the flow is given.

II. BACKGROUND

Stability Theorem

The Stability Theorem enunciated in the Introduction is discussed in Refs [14-18]. Reference [18] gives the Operational Theorem, which is a different enunciate of the Stability Theorem useful for calculating the post stall evolution of the constant-speed line. This Operational Theorem is similar to the Stability-Line hypothesis employed by Ref. [16] to calculate the branch in Fig. 2 with a flow coefficient lower than that of point A. This hypothesis can be summarized as follows. When, based on the Stability Theorem, the operational point is not stable, i.e. when $\xi_c<1$, the blades cannot sustain the flow pattern and the outlet air angle becomes very different from the metal angle fixed

by the geometry of the blades; this deviation increases until a new stable configuration is reached, which, by assuming the premises and the result of the Stability Theorem, is the one that accomplishes ξ_c=1.

For the purpose of this article, it is convenient to remind that Ref. [14] obtains Eq. (1) minimizing a ratio of two well-defined times. This minimization is carried out over the set of all the available experimental arrangements (for a two-dimensional cascade) that can support a given operational point defined by steady and homogeneous inlet and outlet profiles (this configuration is called in Ref. [14] a theoretical flow pattern) in a noisy environment. The Theorem requires as a premise a noisy environment, i.e., it requires the presence of disturbances without specifying the nature (frequency or amplitude) of such disturbances. The required times are the escaping time and the restoring time, which, as it is proved in Ref. [14], can be calculated by using a model based on the integral form of the conservation equations. The calculation of these times also requires to know two characteristic lengths related to the geometry of the rotor, l_θ and l_x. The first characteristic length, l_θ, is the azimuthal length, and the other characteristic length is the axial length, l_x. In the derivation of the stability index, Ref. [14] concludes that l_θ must be equal or inferior to the spacing of the blades and that l_x must be equal or greater than the axial chord of the blades. When, as it was done in Ref. [14], l_θ is taken equal to the spacing of the blades and l_x is taken equal to the axial chord of the blades, the parameter $\sigma_x = l_\theta / l_x$ in Eq. (1) is estimated as the axial solidity of the row, whose expression is given in Eq. (2). However, the derivation in Ref. [14] allows an additional reduction of the azimuthal length that will be used in this paper.

Looking to Fig. 3, it is possible to see that the row defines a characteristic azimuthal length with a lower value than the spacing of the blades. This length is the azimuthal separation between the trailing edge of a blade and the leading edge of the next blade. Therefore, taking the characteristic azimuthal length equal to $l_\theta = 2\pi r / Z - c\sin\beta_m$, where $2\pi r / Z$ is the spacing of the blades, c is the chord of the blade, and β_m is the angle of the blade chord, a new value for the parameter $\sigma_x = l_\theta / l_x$ is obtained (note that $\sigma = 2\pi r / Z / c$ is the solidity of the row):

$$\sigma_x = \frac{\sigma \cos|\beta_m|}{1 - \sigma \sin|\beta_m|} \tag{5}$$

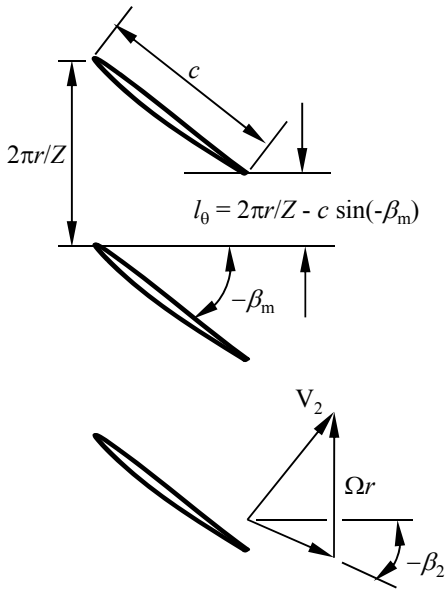

Fig. 3 Characteristic lengths involved in the definition of a row.

Table 1 collects the main angles of the rotor blades used in this paper, taken from Ref. [21]. The last column of Table 1 presents the value of the characteristic parameter σ_x calculated using the Eq. (5). Since the Eq. (4) establishes that the larger the value of σ_x, the larger the stability, it is possible to conclude that the most unstable section of the blade is the one placed at the tip.

Section	r (mm)	$-\beta_1$ (deg.)	$-\beta_2$ (deg.)	$-\beta_m$ (deg.)	σ	σ_x (Eq. 5)
Tip	225.00	57.2	45.6	48.9	0.850	1.554
Mid	191.25	48.8	29.0	36.2	1.000	1.971
Hub	157.50	37.4	5.5	17.9	1.214	1.843

Table 1 Characteristic values at different sections of the blade.

Basic equations

For the purpose of this article, it is convenient to use the following dimensionless variables:

$$u_1 = \frac{V_{x1}}{h_{01}^{1/2}};\ v_1 = \frac{V_{\theta 1}}{h_{01}^{1/2}}$$

$$u_2 = \frac{V_{x2}}{h_{01}^{1/2}};\ v_2 = \frac{V_{\theta 2}}{h_{01}^{1/2}};\ w = \frac{\Omega r}{h_{01}^{1/2}}$$

$$I = \frac{h_{02}}{h_{01}};\ \theta = \frac{h_2}{h_1};\ \Pi = \frac{P_{02}}{P_{01}};\ \chi = \frac{P_1}{P_2}$$

$$a = \frac{A_1}{A_2} \tag{6}$$

Fluid Mechanics imposes six relationships between the dimensionless variables defined in Eqs. (6). (For the sake of simplicity, choke will not be considered in the model.) The work generated by the change of the angular momentum of the flow leads to Eq. (7), the energy equation leads to Eq. (8), the definition of efficiency to Eq. (9), the definition of the total pressure ratio leads to Eq. (10), the continuity equation leads to Eq. (11), and finally, the blade trailing edge to Eq. (12):

$$I = 1 + w(v_2 - v_1) \tag{7}$$

$$\theta = \frac{I - \frac{u_2^{\,2} + v_2^{\,2}}{2}}{1 - \frac{u_1^{\,2} + v_1^{\,2}}{2}} \tag{8}$$

$$\Pi = \left[1 + \eta_R (I - 1)\right]^{\frac{\gamma}{\gamma - 1}} \tag{9}$$

$$\chi = \frac{1}{\Pi}\left(\frac{I}{\theta}\right)^{\frac{n}{n-1}} \tag{10}$$

$$E_1(u_2, v_2) = u_2 - u_1 \chi \theta a = 0 \tag{11}$$

$$E_2(u_2, v_2) = v_2 - w - u_2 \tan \beta_2 = 0 \tag{12}$$

The polytropic exponent in Eq. (10) takes into account the irreversibility in the flow. The definition of the polytropic exponent, in terms of the dimensionless variables given by (6), is:

$$n = \frac{\log \Pi}{\log \frac{\Pi}{I}} \tag{13}$$

The stability coefficient given by Eq. (4) is expressed in terms of the proposed dimensionless variables as:

$$\xi_c = e^{1+\frac{2\theta\left[1-\frac{u_1^2+v_1^2}{2}\right]\left[\chi^{\frac{\gamma-1}{\gamma}}-1\right]}{\left[u_2+\sigma_x|v_2-w|\right]^2}} \tag{14}$$

Given a set of known data $\{u_1, v_1, w, \eta_R, a, \sigma_x, \tan\beta_2, \gamma\}$, it is possible to obtain the set of unknowns $\{u_2, v_2, I, \theta, \Pi, \chi\}$ by substituting $\{I, \theta, \Pi, \chi\}$ given by Eqs. (7-10) into the Eqs. (11) and (12). When this is done, there are two equations $E_1(u_2, v_2)=E_2(u_2, v_2)=0$ and two unknowns. This set of nonlinear equations can be solved with the iterative procedure explained by Ref. [16]. Once the operational point in the map has been completely solved, its stability can be determined by using the Stability Theorem above.

III. EXPERIMENTAL POINTS

In order to check if the new parameters improve the predictions made by Ref. [16], we will use the same axial stage. It consists of a rotor and two cantilevered stators upstream and downstream of the rotor. The basic geometry of the rotor is collected in Table 1. The detailed description of the test rig, experimental facility and instrumentation for this compressor stage can be found in Refs. [19-21] and its schematic is shown in Fig. 4. The angular speed is 1800 rpm [21] so that the expected value for w is 0.06704 (calculated at the mid radius, r = 191.25 mm). The ratio of areas is a=1 (see Fig. 4). The experiments reported by Ref. [20] were conducted for two axial gaps between the rotor and the front stator: the ratios of the gap to the axial chord length at the rotor tip were 1.203 (square points in Fig. 2) and 0.352 (triangle points in Fig. 2). The gap between the rotor and the rear stator was kept to be 1.075 times of the axial chord length. This experimental arrangement is interesting to us because the post-stall evolution of the two configurations is quite different depending on the gap. Ref. [20] reported the evolution of the pressure coefficient (the stage performance comes from the combination of the rotor and the downstream stator), which, is

given in Eq. (15) in terms of the dimensionless variables used in this paper. Note that this equation takes into account an additional loss of total pressure Π_S, which takes into account the ratio of total pressure in the stator.

Ref. [21] describes the stage behavior as follows. For the large gap, at the moment of the stall inception, the flow rate and the pressure rise coefficient decrease by itself from a point where the flow coefficient is near 0.35 to a point where is near 0.32, and the compressor rotor falls into mild stall. When the throttle is closed carefully from the flow coefficient 0.32, the flow rate decreases to a point where the flow coefficient is near 0.30, and then, jumps suddenly to a point where the flow coefficient is near 0.27 and the compressor falls into deep stall. For the small gap, the stall occurs when the flow coefficient reaches the value 0.34, then the flow rate and the pressure-rise coefficient decrease by itself and the compressor falls into deep stall directly in a point where the flow coefficient is 0.28. Therefore, the surge point, point B in Fig. 2, changes from 0.35 to 0.34 depending on the gap. This represents a variation less than 3%. In addition, it is possible to see in Fig. 2 that the small-gap configuration does not present stable operational points in the interval of flow coefficients between 0.26 and 0.31.

$$c_p = \frac{P_{03} - P_{01}}{\frac{1}{2}\rho_1 (\Omega r)^2} = \frac{2}{\left(1 - \frac{u_1^{\,2} + v_1^{\,2}}{2}\right)^{1/(\gamma-1)}} \frac{\gamma - 1}{\gamma} \frac{\Pi\Pi_s - 1}{w^2} \tag{15}$$

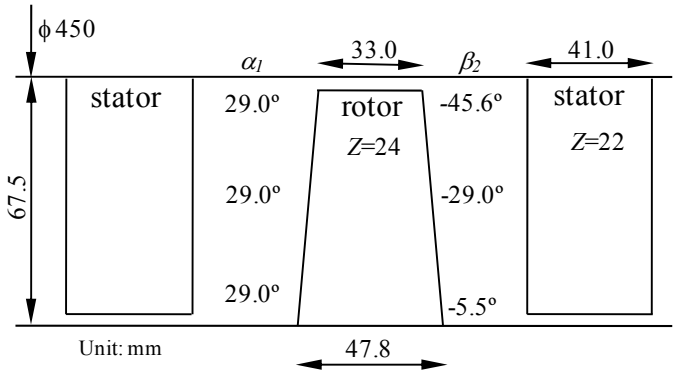

Fig. 4 Schematic view of the segment of the compressor.

Adjustment of the basic equations

For adjusting the basic equations of the fluid dynamics without any influence of the unstable region of the constant-speed line, only the points in the constant-speed line with a flow coefficient greater than 0.425 are used

(see Fig. 5). Four variables of the basic equations are adjusted, the absolute inlet angle of the rotor, the relative outlet angle of the rotor, the efficiency of the rotor, and the total pressure drop in the stator. The result of the least square procedure is collected in Table 2 for both configurations. As can be seen in the last column of Table 2, the variation of the coefficients between both configurations is very small. The rotor efficiency is the parameter that suffers the larger change, but still is less than 1%. The other parameters suffer a variation inferior to 0.5%. The result of this fitting is shown in Figs. 5 and 6. Note that these values are in agreement with the values reported by Ref. [21] because, due to the preceding stator, the absolute flow angle at the rotor inlet has to be near 29.0º ($\tan\alpha_1$=0.55), and the relative flow angle at the rotor exit has to lie in the range from -5.5º at the hub to -45.6º at the tip ($\tan\beta_2$ lies in the range -0.096 to -1.02). Thus, the angles obtained remain near the metal blade angles but, as expected, are not equal because of the deviation. The efficiency of the baseline rotor are reported by Ref. [21], where it is possible to see that the efficiency near the maximum flow rate varies between 0.87 and 0.93. Thus, the values in Table 2 are considered valid for the purpose of this article. It is quite remarkable than the drop of total pressure obtained for the stator 2 does not depend on the size of the gap (see Table 2).

	Large gap	Small gap	Variation
$\tan\alpha_1$	0.4968 (26.4º)	0.4958 (26.4º)	-0.20%
$\tan\beta_2$	-0.3789 (-20.8º)	-0.3780 (-20.7º)	0.24%
η_R	0.8982	0.9052	0.78%
Π_s	0.9950	0.9949	-0.01%

Table 2 Angles and efficiencies for flow coefficients larger than 0.425.

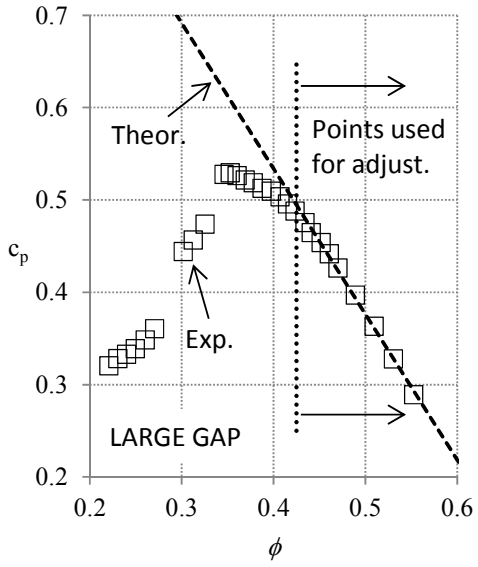

Fig. 5 Theoretical line obtained using the Eqs. (7) to (12) and the values in Table 2 for the large gap.

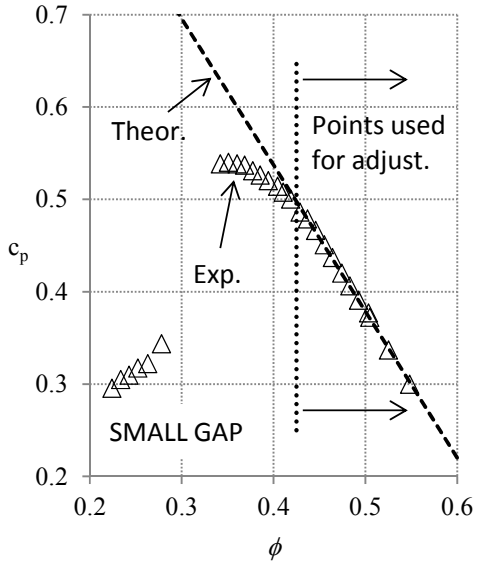

Fig. 6 Theoretical line obtained using the Eqs. (7) to (12) and the values in Table 2 for the small gap.

Since the research in Refs. [19-21] aims to develop an advanced highly loaded axial compressor stage with high efficiency [21], the premises of the Stability Theorem are fulfilled. Thus, if the Stability-Line Hypothesis is used, the stability coefficient given by Eq. (14) can be used to determine the stall inception as well as the averaged post-stall evolution.

The solidity at the tip is $\sigma = 0.850$ and the angle of the chord is $\beta_m = -48.9º$ [21]. Therefore, attending to Eq. (5), the characteristic parameter in Eq. (14) is σ_x=1.5544. Note that the characteristic value used by Ref. [16] was based

on the axial solidity: σ_x=0.56. Obviously, this change in the parameter will produce a change in the prediction of the Stability Theorem. In addition, the value of the exponent in Eq. (10) has been modified with respect to the one used in Ref. [16]. Here, we will use a polytropic exponent calculated, for every operational point, with Eq. (13). Finally, instead of the averaged values for all the mass flow rates used in Ref. [16], we will use for feeding the basic equations of the stage the values written in Table 2. The purpose of this article is to check how these improvements affect the position of the critical points over the constant-speed line (see points B and C in Fig. 2).

IV. PREDICTION OF THE STABILITY THEOREM FOR THE INCEPTION POINT

Using the procedures described by Ref. [16] for solving the Eqs. (7) to (12), we can extrapolate the theoretical constant-speed line for values of the flow coefficient lower than 0.425. Then, Eq. (14) allows us to calculate the stability coefficient along this theoretical line. The result is represented in Fig. 7 for the large gap configuration (geometry and efficiency are fixed by Table 2). In this figure, the dashed line represents those points that exhibit a stability coefficient lower than one. Therefore, according to the Stability Theorem, they are unstable points. The nearest stable evolution, that the Stability Theorem allows, is the one represented by the continuous line in Fig. 7. This supposes a finite change on the slope of the curve just at point C.

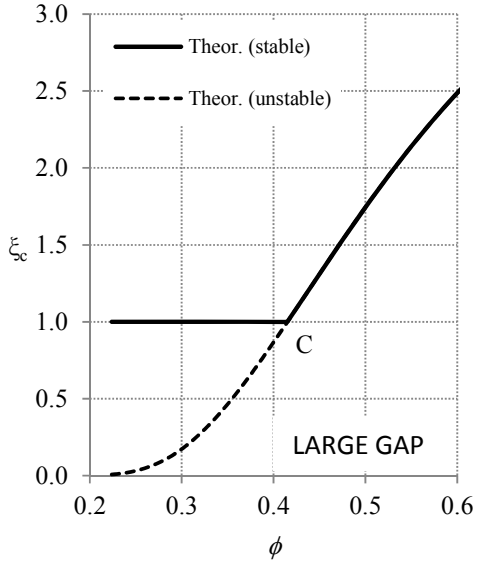

Fig. 7 Stability coefficient for the rotor tip as a function of the flow coefficient.

When the system of Eqs. (7) to (12) produces a value of ξ_c less than one, the Stability Theorem suggests that the equation ξ_c =1 should be added to the system of equations. In this situation there are more equations than unknowns. To solve this problem, Ref. [16] suggests that the relative outlet angle β_2 must be changed. This change allows the relative flow to deflect in order to reach the condition ξ_c =1, and Eq. (12) lets calculate the deviation of the flow. Fig. 8 shows the value of the tangent of β_2 resulting from this calculation. It is possible to see how the value of β_2 remains constant and equal to the value given in Table 2 if the stability coefficient is greater than one, and how the angle changes in order to accomplish with the condition ξ_c =1. The result is a finite change in the slope of the curve. The dashed line represent the values of β_2 leading to the unstable behavior predicted in Fig. 7. Note that for low values of the flow coefficient, the Stability Theorem predicts a large deviation of the flow. Indeed, the relative angle of the stream can reach values as high as -56º, which means a deviation with respect to the guided flow (see Table 2) near -30º. This deviation of the flow is a theoretical result of the basic equations (7) to (12) and the Stability Theorem that imposes the condition ξ_c=1. Section VII will correct this deviation.

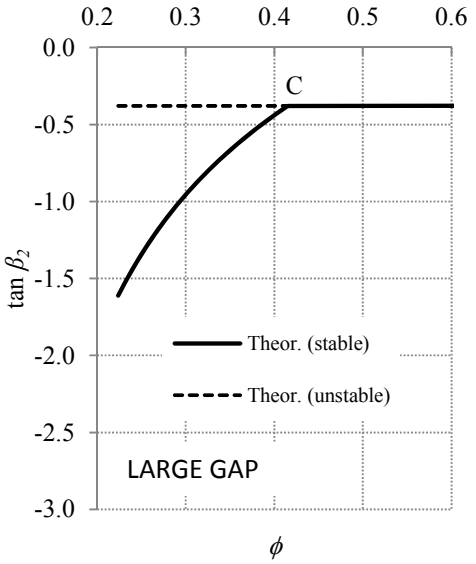

Fig. 8 Relative flow angle at the rotor exit as a function of the flow coefficient.

Therefore, the point C represents a bifurcation in the operational line at constant rotational speed. The theoretical result for the constant-speed line, obtained from the Stability Theorem and the Stability-Line Hypothesis, is the solid line in Figs. 9 and 10 for the large and small gap respectively. Point C in both figures is the flow coefficient where

the value of ξ_c would become less than one. The coefficient flow predicted for the theory at the point where the theoretical-flow-pattern breaks down is 0.4151 for the large gap and 0.4156 for the small gap (predicted values for point C are given in Table 3). Surprisingly, the point where the theoretical flow pattern becomes unstable (point C) is the point where the empirical constant-speed line starts bending. As long as this point is the first one that does not accomplish with the condition ξ_c =1 we will refer to it as the inception point.

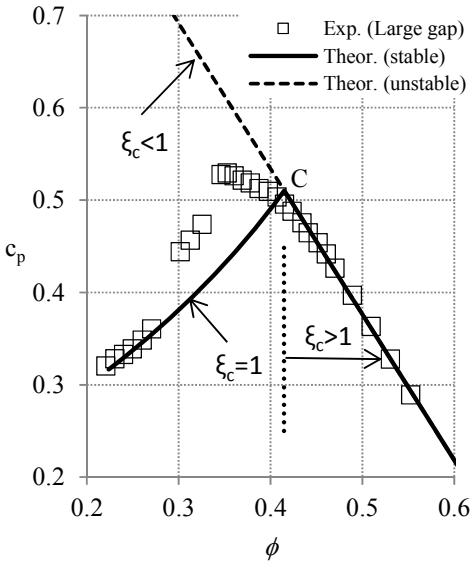

Fig. 9 Pressure coefficient for the large gap configuration as a function of the flow coefficient.

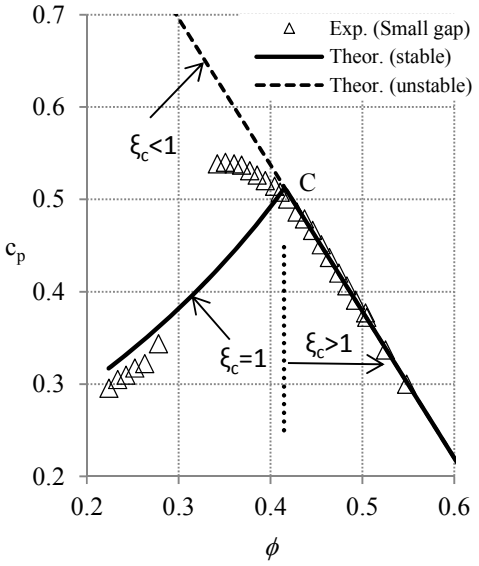

Fig. 10 Pressure coefficient for the small gap configuration as a function of the flow coefficient.

Inception Point (Point C)	LARGE GAP	SMALL GAP	Variation
ϕ	0.4151	0.4156	0.12%
c_p	0.5091	0.5116	0.49%

Table 3 Theoretical prediction of the first point where the theoretical flow pattern becomes unstable.

V. SENSITIVITY ANALYSIS

It is quite interesting to note, that the position of point C predicted by the theory changes less than 0.5% between both configurations and that this variation has the same order of magnitude that the variations in Table 2. In order to see the sensitivity of the position of the critical point with the variables that feed the model, a systematical variation of a 10% has been conducted for the large gap configuration. The results are shown in Table 4, where it is possible to see that the ratio of areas is the parameter that exerts the largest influence on the value of the flow coefficient at the inception point. This result will be used in Section VII. It is worth to mention that the influence of the efficiency is negligible.

$\tan\alpha_1$	$\tan\beta_2$	η_R	Π_S	w	σ_x	a	ϕ	Variation
0.4968	-0.3789	0.8982	0.9950	0.06704	1.5544	1.0	0.4151	0.00%
0.5465	-0.3789	0.8982	0.9950	0.06704	1.5544	1.0	0.4068	-2.00%
0.4968	**-0.3410**	0.8982	0.9950	0.06704	1.5544	1.0	0.4250	2.38%
0.4968	-0.3789	**0.9880**	0.9950	0.06704	1.5544	1.0	0.4153	0.05%
0.4968	-0.3789	0.8982	**0.8955**	0.06704	1.5544	1.0	0.4151	0.00%
0.4968	-0.3789	0.8982	0.9950	**0.07374**	1.5544	1.0	0.4153	0.05%
0.4968	-0.3789	0.8982	0.9950	0.06704	**1.7099**	1.0	0.4069	-1.98%
0.4968	-0.3789	0.8982	0.9950	0.06704	1.5544	**1.1**	0.3847	-7.32%

Table 4 Analysis of sensitivity for the flow coefficient at the inception point.

VI. Influence of the rotor efficiency

The sensitivity analysis has shown that the position of the inception point does not significantly depend on the rotor efficiency. This result surprised us, and hence, we decided to corroborate this idea by looking what values of the rotor efficiency would be required in order to predict the experimental behavior between points B and C. For that

purpose, the efficiency of the rotor (for those points with a value of the flow coefficient lower than 0.425) was adjusted in order to reproduce the experimental constant-speed line also in the post-inception region. To provide that the number of empirical points for all the adjusting variables is enough, the range of interest has been divided in five regions. These divisions have been made trying to retain a similar number of experimental points for every division. Results are in Table 5, where it can be seen that the maximum rotor efficiency is near 98 percent for a flow coefficient near 0.347. This value of the efficiency produces a contradiction with the empirical results reported by Ref. [26] because the maximum measured efficiency that Ref. [26] reported for the controlled-endwall-flow version of this stage is near 93.3 percent at ϕ=0.45. Therefore, we conclude that the efficiency is not directly responsible for the behavior of the constant-speed line between points B and C. This result will allow us to modify the model without changing the values of the efficiency. This will be done in the next section.

Division	Flow Coefficient		Number of experimental points	η_R	Π_S
	from	to			
1	0.200	0.280	6	0.9019	0.9950
2	0.280	0.330	3	0.9543	0.9950
3	0.330	0.365	3	0.9759	0.9950
4	0.365	0.390	3	0.9421	0.9950
5	0.390	0.425	4	0.8985	0.9950
6	0.425	0.550	Previously used	0.8982	0.9950

Table 5 Rotor efficiency that minimizes the error between the theoretical result and the experimental points in Fig. 9.

VII. INFLUENCE OF THE OUTLET DEVIATION ON THE POST-INCEPTION EVOLUTION

As can be seen in Table 4, the ratio of areas is the parameter that produces the maximum variation of the flow coefficient at the inception point. Therefore, it is plausible to think that this parameter has a staple influence on determining the behavior of the constant-speed line between points B and C. The outlet relative angle and the parameter σ_x also affect the position of this point. Indeed, the relative outlet angle has been used in Section IV to "stabilize" the operational line for those flow coefficients with a value lower than the inception one. However, this

cannot be the unique parameter changing. This is a direct conclusion of the previous section because the rotor efficiencies required for explaining the experimental points (with a and σ_x given constants) are much greater than the measured ones, and because, when a and σ_x are fixed, the Stability Theorem requires deviations as large as 30º (see Fig. 8).

When the stability coefficient is equal to one, the escaping particles are just near to disturb the inlet flow. Hence, the Stability Theorem allows us to assume that the escaping particles are deflecting the main flow just until the point where the configuration becomes stable. Under these conditions, it seems also plausible that the outlet area cannot be entirely used by the main flow. In order to check if this hypothesis can explain the shape of the constant-speed line, we will introduce the simplest geometrical model that can reproduce this behavior.

Let us assume that the deflection of the outlet flow is produced by an apparent increment of the blade thickness. In the scope of this paper, this increment of thickness is related to the presence of the escaping particles, but it is out of the scope of this article to discover how the escaping particles produce that effect. It will be the purpose of future works to discover the real mechanism (the deviation could be due to an increment of the boundary layer, due to a modification of the separation point, due to the tip-clearance flow…). According to the scheme in Fig. 11, this effect can be taken into account (without knowing the detailed mechanism) by introducing an apparent metal angle β_m^*. Thus, we assume that the flow is driven by two angles, the actual stagger β_m and the apparent stagger β_m^*. Although this is a rough simplification of the complex flow that appears due to the interaction of the escaping particles and the main flow, it reflects the effect of interest to us. Note that due to geometrical restrictions, the maximum admissible angle for $-\beta_m^*$ is obtained when the straight line defined by $-\beta_m^*$ reaches the trailing edge of the next blade. Let $-\beta_M^*$ be this maximum angle:

$$\tan\left|\beta_M^*\right| = \frac{1+\sigma\sin\left|\beta_m\right|}{\sigma\cos\left|\beta_m\right|} \tag{16}$$

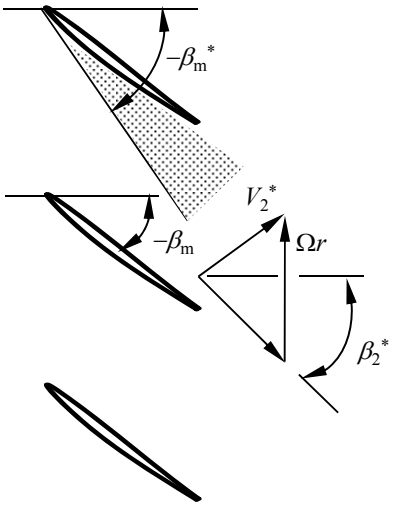

Fig. 11 Geometrical model proposed for taking into account the effect of the outlet deflection in the outlet area and characteristic azimuthal length.

When the flow is well guided, the metal angle β_m drives the flow angle β_2, and when the flow is bad guided the apparent metal angle β_m^* leads to the flow angle β_2^*; hence, it is plausible to assume that, for small changes of the deviation, $\beta_m^* - \beta_m = \beta_2^* - \beta_2$ holds. However, the previous relationship cannot be valid for large deviations because the angle $-\beta_m^*$ cannot be larger than the angle $-\beta_M^*$. The simplest relationship taking into account this limitation is the following one:

$$\beta_m^* = \beta_m + \frac{\beta_2^* - \beta_2}{\frac{\beta_2^* - \beta_2}{\beta_M^* - \beta_m} + 1} \tag{17}$$

Now, this apparent metal angle can be used for recalculating the characteristic azimuthal length as $l_\theta = 2\pi r / Z - c\cos(-\beta_m)\tan(-\beta_m^*)$. Therefore, the apparent outlet area a^* and the new value of the parameter σ_x are:

$$a^* = \frac{a}{1 - \sigma\cos|\beta_m|\left[\tan|\beta_m^*| - \tan|\beta_m|\right]} \tag{18}$$

$$\sigma_x = \frac{\sigma \cos|\beta_m|}{1 - \sigma \cos|\beta_m| \tan|\beta_m^*|} \tag{19}$$

Both, the correction in the area and the new value of σ_x, tend to increase the value of ξ_c. This is because the greater the value of $-\beta_m^*$, the lower the value of both, the outlet area and the characteristic azimuthal length. Hence, the new model tends to reduce the deviation required to accomplish with the condition $\xi_c = 1$. Taking into account this simple model, a new calculation of the constant-speed line can be done. The result is shown in Fig. 12 for the large-gap configuration (the result for the small-gap configuration is similar).

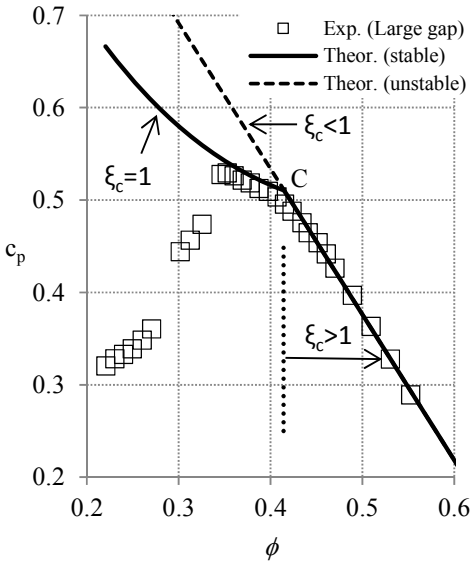

Fig. 12 Operational line calculated with the geometrical model of Fig. 11.

The solid line in Fig. 12 has been obtained with a constant value of the rotor efficiency and stator pressure drop (equal respectively to 0.8982 and 0.9950, that are the values fixed by the non-stall straight part of the constant-speed line). It is possible to see how the new line in Fig. 12 follows the tendency that the experimental points exhibit. Figure 13 shows the deviation of the flow needed for reaching the condition ξ_c=1. The new deviation is significantly lower than the previous one (compare Figs. 8 and 13). In this case, the relative angle of the stream reaches a maximum value of -31º, which means a deviation respect to the guided flow (see Table 2) near -10º.

The new geometry of the flow "stabilizes" the operational point over the empirical constant-speed line and hence, this result allows us to conclude that this basic model retains the dominant effects related to the behavior of

the constant-speed line between points B and C. The next section will show that the position of the surge point, point B, is also related to the Stability Theorem.

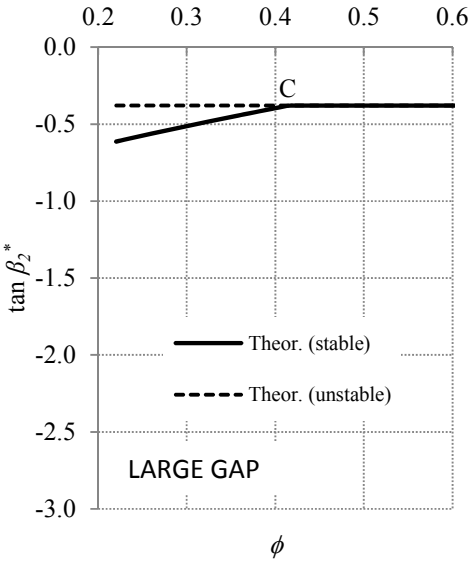

Fig. 13 Corrected flow angle at the rotor exit as a function of the flow coefficient.

VIII. INFLUENCE OF THE INLET INCIDENCE ON THE DETERMINATION OF THE SECOND CRITICAL POINT

In the previous calculations we have assumed that the escaping particles are generated by the tip region of the blades because it is the section with a lower value of σ_x. However, it is plausible to think that these escaping particles are able to induce new escaping particles in other sections of the blades next to the tip. Thus, the escaping particles can become a majoritarian component of the flow if a large section of the blade near the tip exhibits a value of ξ_c near one. Since the condition ξ_c=1 means that the escaping particles have the potential to reach the inlet region, it is plausible that the distortions eventually generated by the escaping particles in the outlet region affect significantly the inlet region. Since the main flow is calculated with the mid radius, we assume that the escaping particles dominate the flow when they are able to disturb the inlet section just in the middle section of the blade. (Attending to the values in Table 1, the mid radius has a solidity equal to 1.000 and a stagger equal to -36.2º with a value σ_x = 1.971.) To check this idea, Fig. 14 shows the calculated values of ξ_c for the tip and the mid radius using the constant-speed line calculated in the previous section. Table 6 shows the predicted values of the surge point for the large and small gap configurations.

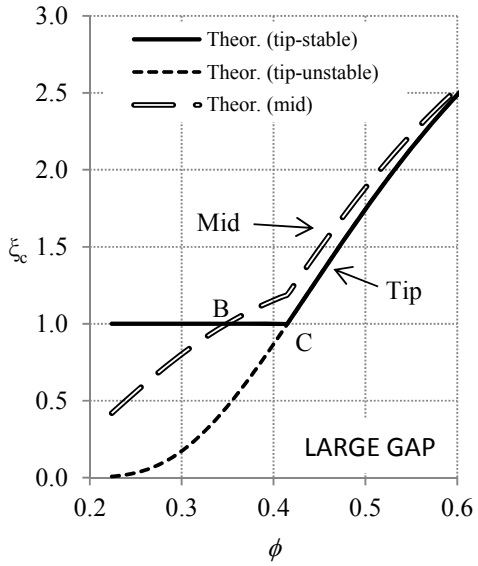

Fig. 14 Stability coefficient for the tip and mid sections as a function of the flow coefficient.

Fig. 14 shows that although the mid-section of the blades is more stable than the tip section for high values of the flow coefficient, finally the stability coefficient of the mid-section drops below one. This happens for a flow coefficient near $\phi = 0.3494$ (point B in Fig. 14). Note that the mid section becomes unstable even taking into account the deviation of the flow required to maintain the stability of the tip section. Attending to the Stability Theorem, this means that the mid-section cannot sustain a theoretical flow pattern for lower values of the flow coefficient. Thus, there are escaping particles in the inlet region of the mid-section of the blades and hence, it is plausible to think that the inlet area is also reduced. The main consequence of this fact is that Eq. (18) cannot be longer valid, and must be substituted again by $a^*=a=1$. When this change is done, the deviation of the flow is given by the solid line in Fig. 15, and the constant-speed line by the solid line in Fig. 16.

	LARGE GAP			SMALL GAP		
Surge Point (Point B)	Theor.	Exp.	Variation	Theor.	Exp.	Variation
ϕ	0.3494	0.35	0.17%	0.3498	0.34	2.88%

c_p	0.5429	0.53	2.43%	0.5102	0.54	5.52%

Table 6 Theoretical prediction for the first point where the mid section of the blade becomes unstable.

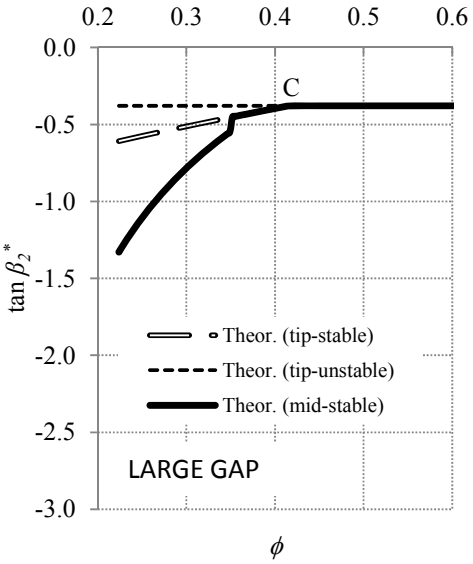

Fig. 15 Corrected relative flow angle at the rotor exit as a function of the flow coefficient required for stabilizing the mid section.

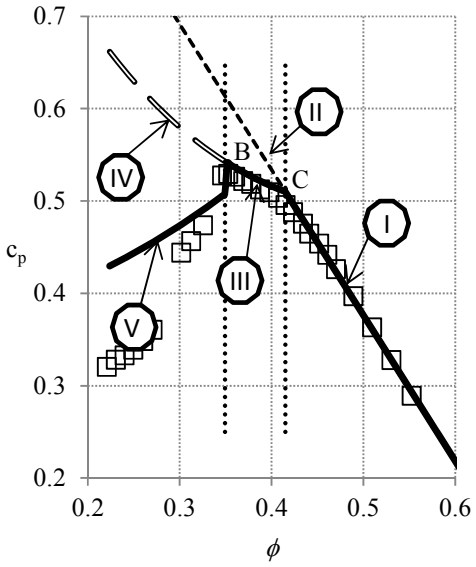

Fig. 16 Pressure coefficient as a function of the mass flow rate. The different branches are the different theoretical solutions obtained attending at the value of the stability coefficient at the tip and mid sections (see Table 7).

The important regions in Fig. 16 have been numerated from I to V according to its order of apparition when the flow coefficient is reduced. Fig. 17 shows the different values of the stability coefficient and Table 7 collects the main features of every region. For high values of the flow coefficient, both, the tip and the mid sections have a value of the stability coefficient greater than one and there is not a significant deviation of the flow. When the flow coefficient at point C is reached, the stability coefficient of tip section reaches the value one. At this point a bifurcation appears. If the deviation of the flow is not modified, the constant-speed line evolves along the region II. However, this part of the line has values of the stability coefficient lower than one, and hence cannot be sustained. If a greater deviation of the flow is assumed (in order to keep the stability coefficient at the tip section equal to one), the constant-speed line evolves as line III indicates. Note that in this part of the line the reduction of area and azimuthal length is enough to keep the stability coefficient of the mid section larger than one. However, when the flow coefficient is reduced towards the point B, the stability coefficient at the mid section reaches the value one, and hence, any further reduction of the flow coefficient following the line IV produces a stability coefficient of the mid section lower than one. This fact avoids following the line IV. At this point, the inlet section is severely perturbed by the escaping particles and the inlet area is drastically reduced. To overcome this reduction of the area, the deviation of the flow has to increase drastically. This effect produces the drop of the pressure ratio that appears just at the point B and that is experimentally observed in Fig. 16. The result is that the constant-speed line evolves following line V. However, with the new value of the inlet area the tip section becomes unstable because the sudden increment of the deviation is not enough to stabilize this section. Under this condition, the deviation required to stabilize the tip section is the one drawn in Fig. 8, that cannot be actually obtained because it requires higher rotor efficiencies than the ones allowed by the configuration (see Section VI). In this part, the Stability Theorem is not completely conclusive because the stabilization of one section destabilizes the other section (the last grey row of Table 7 summarizes this fact).

REGION	Reduction of area	ξ_c(tip)	ξ_c(mid)	Flow pattern
I	NO ($-\beta_m^* = -\beta_m$; a=1)	>1	>1	Theoretical Flow Pattern.
II	NO ($-\beta_m^* = -\beta_m$; a=1)	<1	>1	Inlet section perturbed by reversed flow at the tip.
III	YES ($-\beta_m^* > -\beta_m$; a>1)	=1	>1	Inlet section slightly perturbed by reversed flow at the tip.
IV	YES ($-\beta_m^* > -\beta_m$; a>1)	=1	<1	Inlet section perturbed by reversed flow at the mid.
V	NO ($-\beta_m^* = -\beta_m$; a=1)	<1	=1	Inlet section perturbed by reversed flow at the tip.
V	YES/NO	~1	~1	Unsteady behavior and/or a mixed behavior between the lines IV, V and the solid line in Fig. 7.

Table 7 Behavior of the stability coefficient at tip and mid sections for every line in Fig. 16.

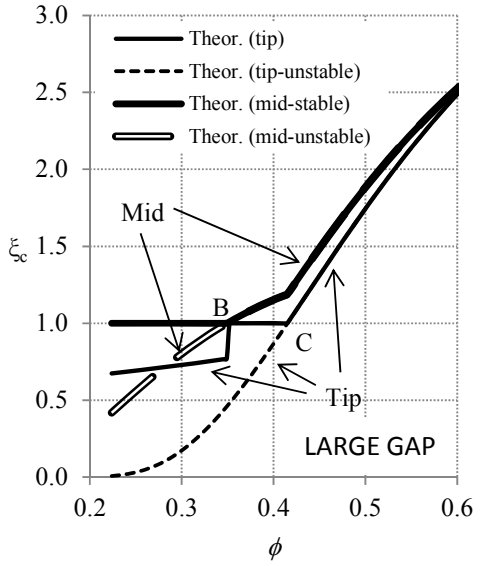

Fig. 17 Stability coefficient for the tip and mid sections as a function of the flow coefficient. The solid lines give the evolution of the stability coefficient for the tip and mid sections over the branches I, III and V in Fig. 16.

Finally, in order to check that the solution given by lines I, III and V in Fig. 16 is not incompatible with the efficiency, the rotor efficiency has been adjusted anew. The values of the new values of the rotor efficiency are collected in Table 8. Although the values of the rotor efficiency do not exactly coincide with the ones reported by Ref. [26], they are not incompatible.

Division	Flow coefficient		Number of experimental points	η_R	Π_S
	from	to			
1	0.200	0.280	6	0.8120	0.9950
2	0.280	0.330	3	0.8787	0.9950
3	0.330	0.365	3	0.8981	0.9950
4	0.365	0.390	3	0.8912	0.9950
5	0.390	0.425	4	0.8901	0.9950
6	0.425	0.550	Previously used	0.8982	0.9950

Table 8 Rotor efficiency that minimizes the error between the theoretical result and the experimental points.

IX. DISCUSSION

The second critical point that the Stability Theorem predicts is point B, the surge point, which attending to the calculus occurs when the flow coefficient is equal to 0.3494. The experimental value reported by Ref [21] is near 0.34 or 0.35 depending on the gap, which means an error inferior to 5%. It is a surprise that a geometrical model, based on calculating an apparent outlet flow area and a characteristic value σ_x, gives such a good estimation. However, we explain this fact attending to two factors: 1) the rotor under study is a low Mach number compressor, and 2) the staple ingredients that are required to lead the rotor to the surge inception are included in the Stability Theorem.

The Stability Theorem establishes a change in the behavior of the constant-speed line when the inlet section is surpassed by escaping particles without entering in discussing what mechanism is leading to those escaping particles. Indeed, one of the premises of the Stability Theorem is the necessity of noises. These noises have to be as large as possible to produce the escaping particle when the thermodynamics and the kinematics allow this fact. The theory shows that the compressor under study in this work has two points where the escaping particles generated by the noises are able to reach the inlet station: the inception point (point C) and the surge point (point B). The response of the flow pattern to this disruption of the inlet section consists basically in a loss of guidance of the flow. This change in the angle of the flow respect to the metal angle of the blades also modifies the ratio of areas and the

characteristic lengths of the blades that the mean flow "sees". This situation can be considered as a quasi-steady configuration as long as the Stability Theorem can be fulfilled with a value of the stability coefficient equal to one. This is the expected behavior in the region dominated by lines I and III in Fig. 16. The expected flow patterns in those regions can be schematized as Fig. 11 shows. However, when the flow coefficient is reduced below the surge point, the mid section of the stage reaches a value of the stability coefficient lower than one. Any attempt for stabilizing this section produces a destabilization of the tip section and vice versa. Therefore, the flow pattern over the line V in Fig. 16 should be much more complicated. Probably, the mechanism in that area is not quasi-steady. If this is the case, there must be a natural fluctuation of the properties of the flow and the observed response should be a dynamic phenomenon. In addition, attending to the Stability Theorem, this should happen with independence of the kind of disturbances, and hence, this temporal evolution should not be correlated with external characteristic times or frequencies. This could explain why it is not easy to identify a stall-inception mechanism based on external frequencies. The difficulties associated to the identification of the stall-inception mechanism are well explained by Day et al. [24].

Assuming that the Stability Theorem holds, we can conclude that a temporal and spatial average of the flow pattern at the surge point has to exhibit reversed flow near the inlet region of the tip rotor and a significant deviation of the flow. Although it is out of the scope of this paper to discover the inner structure of the flow, we imagine this flow pattern as the one roughly drawn in Fig. 18. In this figure, the thickness and the length of the blades is increased by the reversed flow. The result is that the grey area in that picture is not accessible to the main flow. This feature is indirectly supported by the experimental results obtained by Ref. [21] when the gap between the preceding stator and the rotor is changed. In the configuration with a large gap there are experimental points in the region near a flow rate of 0.32 [21], but those points disappear when the gap is reduced (see experimental points in Figs. 5 and 6). Here we can explain this experimental fact by stating that the presence of the previous stator interferes with the flow pattern required for stabilizing the flow. If the preceding stator does not allow the flow to deflect as it is shown by the dashed lines in Fig. 18, the operational point cannot be stabilized. Consequently, due to the unstable character of these operational points, the flow pattern will not be a steady and homogeneous one, so that the stability theorem cannot be conclusive about the final flow pattern. However, it is conclusive when it states that the flow pattern in such situation is not a theoretical flow pattern. In this region Greitzer's theory [22,23] can be applied to obtain the

post-stall evolution of the entire system, because, as Greitzer explains, the behaviour of the system depends on the system configuration.

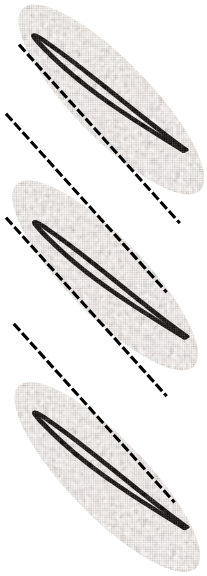

Fig. 18 Schematic of the basic geometry used to explaining the behavior in the post-surge constant-speed line.

7. CONCLUSIONS

A new way to calculate the outlet area and the azimuthal characteristic length of a row of blades has been proposed for feeding the calculation of the stability coefficient. An important result is that the characteristic azimuthal length affecting the stability of the constant-speed line is less than the spacing of the blades. Indeed, it is shown that the stagger angle of the blades must be used to calculate this characteristic length. As a result, the Stability Theorem predicts two points where the constant-speed line of an axial rotor bifurcates. The first point is the inception point and the second one is the surge point. The inception point is determined by the presence of escaping particles in the inlet section at the tip radius of the rotor. The surge point is determined by the presence of escaping particles in the inlet section at the mid radius. The ability of the model to capture the observed behavior has been assessed against experimental results. In particular, the flow coefficient where the surge occurs has been theoretically determined with an error level lower than 5 percent. The procedure has predicted the correct pressure ratio of the constant-speed line between the inception and surge points and gives a qualitative description of the shape of the constant-speed line once the surge point has been surpassed. In addition, it predicts the abrupt drop of the pressure ratio in the surge point and the positive slope of the constant-speed line beyond the surge point. An

analysis of sensitivity has shown that the rotor efficiency has little influence on determining the flow coefficients of inception and surge points and that the most relevant parameter is the ratio of areas, which is controlled by the deviation of the flow. The following additional conclusions were deduced from the study:

1 The Stability Theorem holds true over the entire constant-speed line, not only for the bifurcation point. This allows the adoption of a completely new model for the deviation of the air flow angle and related geometry.

2 The stability coefficient is correlated with the size of the regions subjected to flow separation. Where the stability coefficient is much lower than one, the model requires large flow separation.

3 Provided that a noisy environment is present, the point at which instability occurs does not depend on the kind of the disturbances. This point is set with independence of the mechanism adopted for calculating the evolution of the amplitude of the disturbances and hence, with independence of its wavelength or frequency.

Acknowledgment

This work has been partially supported by a grant from Fundación Caja Madrid (2011-2012).

Notation

a = ratio of inlet to outlet area $=A_1/A_2$
A = annular area
c = chord
c_p = pressure coefficient
E = equation
h = enthalpy
I = total to total enthalpy ratio $=h_{02}/h_{01}$
l = characteristic length
P = pressure
r = radius
u = absolute axial velocity divided by $h_{01}^{1/2}$
v = absolute tangential velocity divided by $h_{01}^{1/2}$
V = absolute velocity of air
w = blade speed divided by $h_{01}^{1/2}$
Z = number of blades
α = absolute flow angle measured from the axial direction
β = relative (to the rotor) flow angle measured from the axial direction
χ = ratio of inlet to outlet static pressure $=P_1/P_2$
Δ = dimensionless parameter defined by Eqs. (1) and (5)
ϕ = flow coefficient (axial velocity/blade speed)
Φ_{esc} = potential for escaping
γ = ratio of specific heats
η = adiabatic efficiency
Π = stagnation pressure ratio

θ = static enthalpy ratio = h_2/h_1
ρ = density
σ = solidity (chord/spacing ratio)
Ω = angular speed of the rotor
ξ = stability margin coefficient
ξ_c = stability coefficient

Subindexes

x = axial component
R = rotor
S = stator
θ = azimuthal component
0 = stagnation conditions
1 = inlet conditions
2 = outlet conditions

All the equations are derived with a constant radius assumption and air is treated as a perfect gas with constant specific heats.

References

1 Hoying, D.A., Stall Inception in a Multistage High-Speed Axial Compressor, Journal of Propulsion and Power, Vol. 11, no. 5, 1995, pp.915-922

2 Dhingra, M., Neumeier, Y., and Prasad, J.V.R., Stall and Surge precursosrs in Axial Compressors, AIAA 2003-4425

3 McDougall, N.., Cumpsty, N.A., and Hynes, T.P., Stall Inception in Axial Compresors, Journal of Turbomachinery, Vol. 112, 1990, pp. 116-125

4 Sane, .K., and Tagade, P., Effect of Rotor Solidity on Stall Inception and Growth in Axial Flow Fan, AIAA 2004-3550

5 He, L., Computational Study of Rotating-Stall Inception in Axial Compressors, Journal of Propulsion and Power, Vol. 13, no. 1, 1997, pp. 31-38

6 Gogoi, A., Verma, S., Sane, S.K., A Model for Rotating Stall and Surge in Axial Flow Compressors, AIAA 2002-4086

7 Markopoulus, N., Neumeier, Y., Prasad, J.V.R. and Zinn, B.T. An Extended Analytical Model for Compressor Rotating Stall and Surge. In 35th AIAA Joint Propulsion and Exhibit, Los Angeles, California, AIAA-99-2124, 20-24 Jun. 1999

8 Longley, J.P., Calculating Stall and Surge Transients, ASME Turbo Expo 2007: Power for Land, Sea and Air, May 14-17, 2007, Montreal, Canada

9 Wang, H., Hennecke, D.K. and König, A., Method for Estimating Various Operating States in a Single-Stage Axial Compressor, Journal of Propulsion and Power, Vol. 11, no. 2, 1995, pp.385-387

10 Koch, C.C., Stalling Pressure Rise Capability if Axial Flow Compressor Stages, Journal of Engineering for Power, Vol. 103, 1981, pp. 645-656

11 Benavides, E. M., Tizón, J. M. and Juste, G. L. Theoretical Formula for Quick Selection of the Number of Blades in Designing Axial-Flow Compressors. International Journal of Turbo and Jet Engines, Vol. 24, 2007, pp. 63, 73

12 McCaughan, F.E. Bifurcation Analysis of Axial Flow Compressor Stability. SIAM Journal on Applied Mathematics, Vol. 50, No. 5, Oct. 1990, pp. 1232, 1253

13 N.A. Cumpsty, *Compressor Aerodynamics*, Krieger Publishing Company, Malabar, Florida, 2004

14 Benavides, E. M., Theoretical characterization of stability in axial-flow compressor rotors, Proc. IMechE Part G: J. Aerospace Engineering, vol. 223, 2009.

15 Benavides, E.M., "Method and device for predicting the instability of an axial compressor", WO 2011020941 (A1) , Application number: WO2010ES70563 20100820, Priority number(s): ES20090030614 20090821

16 Benavides, E.M., "On the theoretical calculation of the stability line of an axial-flow compressor stage", International Journal of Turbo and Jet Engines, 2011, Freund Publishing House Ltd.

17 Benavides, E.M., "Theoretical calculation of stability for NASA Stage 57 rotor", International Journal of Turbo and Jet Engines, 2009 Vol. 26, pp. 87-95, Freund Publishing House Ltd.

18 Benavides, E.M., Juste, G.L., "Theoretical calculation of stability for NASA Stage 57 stator", International Journal of Turbo and Jet Engines, 2011, Vol 28, DOI 10.1515/TJJ.2011.022; Freund Publishing House Ltd.

19 Inoue, M., Kuroumaru, M., Yoshida, S. And Furukawa, M., Short and Long Lenght-Scale Disturbances Leading to Rotating Stall in an Axial Compressor Stage with Different Stator/Rotor Gaps, ASME J. Turbomachinery, Vol. 124, pp. 2002, 376-384

20 Inoue, M., Kuroumaru, M., Tanino, T. and Furukawa, M., Propagation of Multiple Short-Lenght Scale Stall Cells in an Axial Compressor Rotor, Journal of Turbomachinery, Vol. 122, 2000, pp. 45-54.

21 Inoue, M., Kuroumaru, M., Furukawa, M., Kinoue, Y., Tanino, T., Maeda, S. and Okuno, K., Controlled-Endwall-Flow Blading for Multistage Axial Compressor Rotor, ASME Paper, no. 97-GT-248, 1997, pp. 1-11

22 Greitzer, E.M. Surge and Rotating Stall in Axial Flow Compressors. Part I: Theoretical Compression System Model. Engineering for power, Vol. 98, No.2, 1976, pp. 190, 198.

23 Greitzer, E.M. Surge and Rotating Stall in Axial Flow Compressors. Part II: Experimental Results and Comparison with Theory. Engineering for power, Vol. 98, No.2, 1976, pp. 199, 211

24 Day, I.J., Breuer, T. Escuret, J., Cherrett, M. and Wilson, A., Stall Inception and the prospects for active control in four high speed compressors, ASME J. Turbomachinery, Vol. 121, pp. 18-27